PL-TR-92-2174

ANALYSIS OF IBSS SPECTRA OF SPACE SHUTTLE CONTROL ENGINE EXHAUST

D. L. A. Rall
I. L. Kofsky

PhotoMetrics, Inc
4 Arrow Drive
Woburn, MA 01801-2067

31 May 1992

Scientific Report No. 1

PHILLIPS LABORATORY
AIR FORCE SYSTEMS COMMAND
HANSCOM AIR FORCE BASE, MA 01731-5000

This technical report has been reviewed and is approved from publication.

TERRY L. THIEM, Capt, USAF
Contract Manager

CHARLES P. PIKE, Branch Chief
Spacecraft Interactions Branch

This document has been reviewed by the ESC Public Affairs Office (PA) and is releasable to the National Technical Information Service (NTIS).

Qualified requestors may obtain additional copies from the Defense Technical Information Center. All others should apply to the National Technical Information Service.

If your address has changed, or you wish to be removed from the mailing list, or if the addressee is no longer employed by your organization, please notify PL/TSI, Hanscom AFB, MA 01731-5000. This will assist us in maintaining a current mailing list.

Do not return this report unless contractual obligations or notices on a specific document requires that it be returned.

DISCLAIMER NOTICE

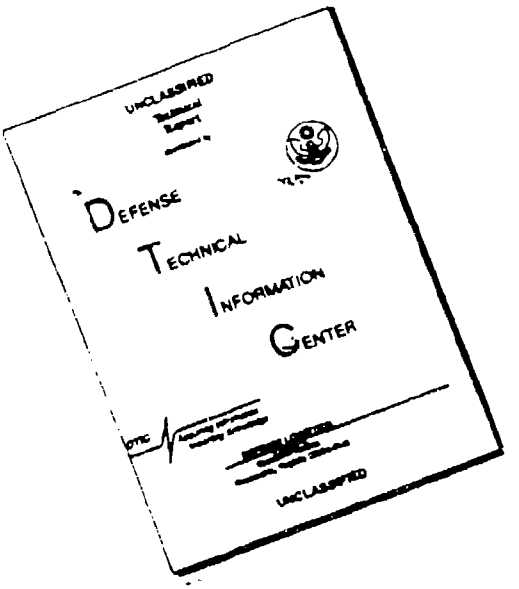

THIS DOCUMENT IS BEST QUALITY AVAILABLE. THE COPY FURNISHED TO DTIC CONTAINED A SIGNIFICANT NUMBER OF PAGES WHICH DO NOT REPRODUCE LEGIBLY.

REPORT DOCUMENTATION PAGE

Form Approved
OMB No 0704-0188

1 AGENCY USE ONLY *(Leave blank)*	2 REPORT DATE	3 REPORT TYPE AND DATES COVERED
	31 May 1992	Scientific Report No. 1

4 TITLE AND SUBTITLE
Analysis of the IBSS Spectra of Space Shuttle Control Engine Exhaust

5 FUNDING NUMBERS
PE 62101F
PR 7610 TA 30 WVCP

Contract No.
F19628-91-C-0061

6 AUTHOR(S)
David L. A. Rall
Irving L. Kofsky

7 PERFORMING ORGANIZATION NAME(S) AND ADDRESS(ES)
PhotoMetrics, Inc.
4 Arrow Drive
Woburn, MA 01801-2067

8 PERFORMING ORGANIZATION REPORT NUMBER

9 SPONSORING/MONITORING AGENCY NAME(S) AND ADDRESS(ES)
Phillips Laboratory
Hanscom AFB, MA 01731-5000

Contract Manager: Capt T. Thiem/WSSI

10 SPONSORING/MONITORING AGENCY REPORT NUMBER
PL-TR-92-2174

11 SUPPLEMENTARY NOTES

12a DISTRIBUTION/AVAILABILITY STATEMENT
Approved for Public Release:
Distribution Unlimited

12b DISTRIBUTION CODE

13 ABSTRACT *(Maximum 200 words)*

Infrared Background Signature Survey spectra of exhaust gases from attitude controlling liquid-bipropellant thrusters, taken from onboard space shuttle on mission STS-39 in connection with the Orbiter Environment Experiment, are analyzed. The high-resolution multichannel sensor viewed both the expanding combustion products near the engine and through the volume where these high kinetic energy molecules react with atmospheric species. Its segments of data over about half the spectrum range between 2.5 and 17.5 μm showed primarily H_2O and CO_2 vibrational and rotational radiation, with no other emission features unambiguously identifiable. A comparison with synthetic spectra compiled from HITRAN gave a reasonably close fit to excited-state temperatures 800 - 1200K, while the absolute radiances were in some cases below those that would result from the column-concentrations of exhaust species predicted by CONTAM because of collision limiting. These spectral radiances quantify the optical contamination resulting from Shuttle Orbiter's routine reaction control engine firings.

14 SUBJECT TERMS
Infrared Background Signature Survey
Liquid Bipropellant Rocket Exhaust Spectra
Infrared Emission from H_2O and CO_2

15 NUMBER OF PAGES
30

16 PRICE CODE

17 SECURITY CLASSIFICATION OF REPORT	18 SECURITY CLASSIFICATION OF THIS PAGE	19 SECURITY CLASSIFICATION OF ABSTRACT	20 LIMITATION OF ABSTRACT
Unclassified	Unclassified	Unclassified	SAR

TABLE OF CONTENTS

LIST OF FIGURES

LIST OF TABLES

ANALYSIS OF IBSS SPECTRA OF SPACE SHUTTLE ENGINE EXHAUST

Introduction

The Infrared Background Signature Survey spectrometer (IBSS, Ref 1) measured intensities of optical-contaminant radiation produced by the exhaust of space shuttle's Primary Reaction Control System (PRCS) thrusters, as part of the AF Phillips Laboratory-directed Orbiter Environment Experiment (E. Murad/WSSI, Principal Investigator). Shuttle Orbiter was at 240 km altitude in a standard nose-down and starboard wing-to-ram flight orientation on day 6 of mission STS-39 (04 May 1991), at 54°S-85°W in the dark hemisphere. The narrow field of view infrared sensor was positioned at the fully upward-extended end of the spacecraft's Remote Manipulator System near the crew cabin end of its payload bay, viewing toward the exhaust volumes of routinely-operating aft aspect-controlling engines as diagrammed in Fig. 1.

The high-resolution data in five spectrum segments covering somewhat less than half of the 2.5-17.5 μm wavelength region showed primarily (perhaps exclusively) vibrational and rotational features of H_2O and CO_2, which are known to be major infrared-active combustion product species; these are summarized in Fig. 13. The issue of the relative contributions to the signal from *1)* thermal excitation of these molecules in the rapidly-expanding and -cooling --and perceivedly out of thermal equilibrium--exhaust gas itself and *2)* collisional excitation as these high-velocity molecules interact with the orbital atmosphere, is not yet fully resolved from the spectra. A further mechanism *3)* of excitative reactions mediated by the nearby surface of Shuttle Orbiter's vertical stabilizer (and its other exposed surfaces) appears a much less probable radiation source, for the reasons stated below. The spatially widespread visible chemiluminescence from collisional excitation at two scale heights lower ambient air densities has recently been characterized from groundbased video camera (Ref's 2, 3) and spectrographic (Ref 4) data, and complements the measurements of this "foreground" that would contaminate infrared remote sensing or surveillance from onboard the spacecraft (a primary purpose of the Orbiter Environment Experiment).

Instrument Pointing

Each of the twelve individual photodetectors in the slit image plane of the wavelength-scanning spectrometer has the same 0.6° by 0.07° rectangular field of view, whose intercept on the visible light-emitting exhaust (-interaction) region in the 12° × 16° rectangular field of a coaligned intensified video camera is indicated at top left of Fig. 1. This infrared line of

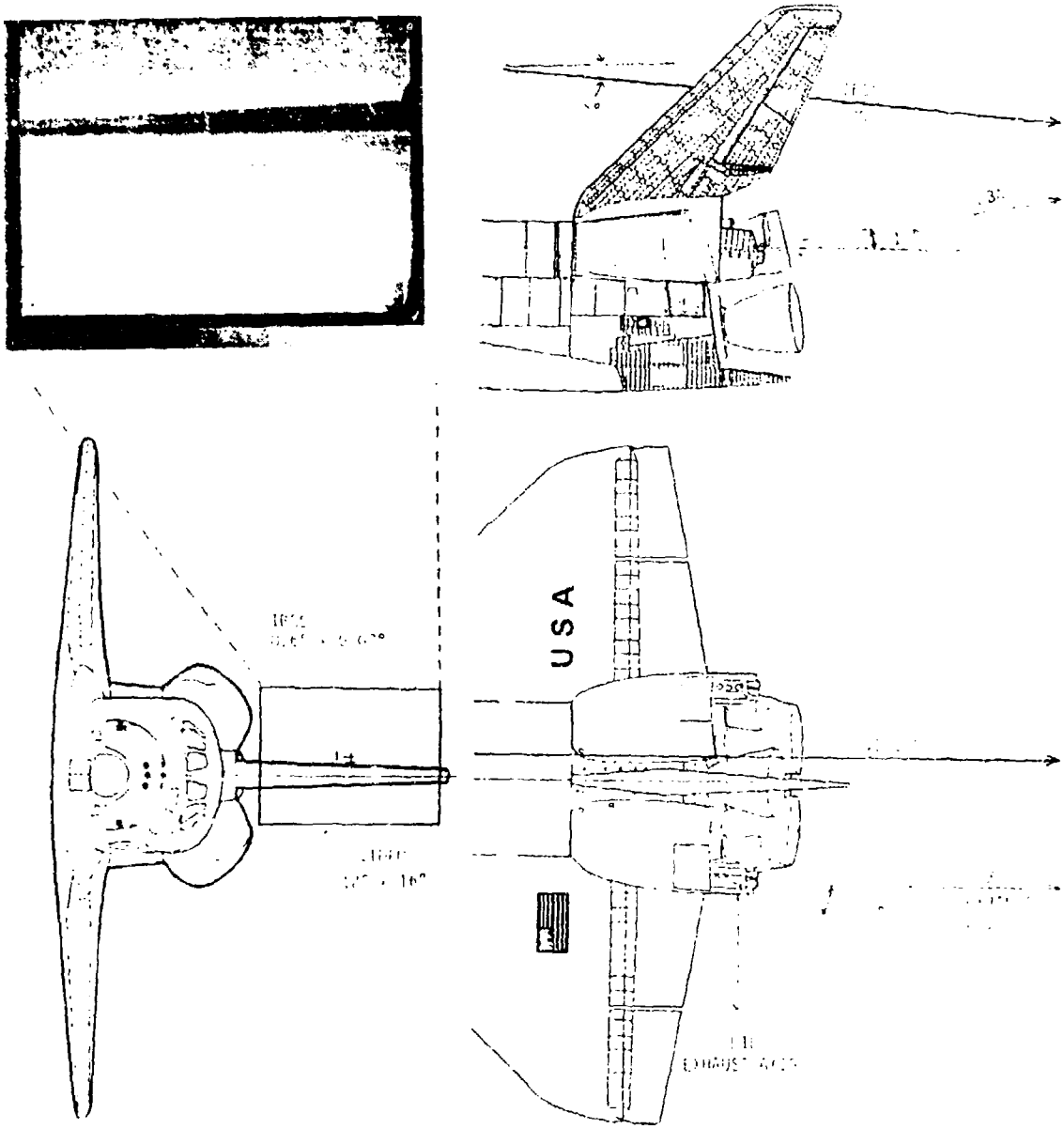

Figure 1. Orthographic projection drawings showing the IBSS pointing vector relative to the shuttle body and the exhaust cones of the two aft PRCS engines. An image from the intensified video camera coaligned with the spectrometer (and with optic axis offset horizontally from it by 50 m) locates the pointing of the $0.07^{\circ} \times 0.6^{\circ}$ field of view instrument during the data period.

sight was at 5° depression from the "X" axis (horizontal in conventional space shuttle coordinates) of Orbiter, clearing the starboard--ram-directed--side of its vertical stabilizer by approximately 0.5° or 15 cm. The sensor itself was located 320 inches (8.1 m) in the Z direction above the floor of the payload bay, at Y = +19 inches (50 cm) starboard from the spacecraft's long symmetry axis and some 17 m horizontally from the aft engine pods.

A 50 cm lateral (-Y-direction) physical offset of the optic axis of the video camera from the spectrometer correspondingly displaces the two lines of sight, so that radiations originating from close to the engine exhaust planes would appear somewhat displaced relative to the narrow-field instrument (the effect becomes negligible in the exhaust-interaction region *2)*). A similar 30 cm vertical (Z-direction) offset between the two axes is to some extent compensated by a -0.6° (downward in the vehicle frame) tilt of a nodding mirror in the IBSS optical system. Rejection of out-of-field infrared radiations by this specially designed sensor is sufficiently high to prevent leakage from the nearby thermally-radiating vertical stabilizer from contaminating its spectra, as is further evidenced by the absence of (graybody) continuous background in the data from this experiment.

Exhaust Direction and Region

Known stars in the field of view of the coaligned video camera confirmed that the aft-viewing IBSS line of sight was almost directly into the zenith (that is, away from the "hot" hard earth and atmosphere), and indeed the spectral scans showed negligible thermal signal in the periods when no PRCS engines were operating. A MSIS atmosphere-model calculation gave densities of atomic oxygen and of all atmosphere species at the altitude and geophysical conditions of the STS-39 experiment as 2.5×10^9 cm^{-3} and 3.5×10^9 cm^{-3} respectively, and collision mean free path of ambient species 500 m (in the "hard-sphere" definition of the US Standard Atmosphere). At these low orbital densities no identifiable air "shock" region develops (although the local air density is to some extent depleted); the exhaust gas intermixes with the atmosphere broadly as described in Ref 5.

Each of the firings investigated was of a combination of the rocket motors in the left aft PRCS pod identified as L1L and L3A; refer again to Fig. 1. As the former thrusts in directions largely parallel to the portside or -Y direction (and thus into Orbiter's wake) virtually all of its adiabatically-expanding exhaust, and the principal volume in which this gas produces radiation as it reacts with the orbital atmosphere (process *2)* above), would lie outside the IBSS field. The latter engine thrusts aft at 10° elevation from the spacecraft's X axis, closely perpendicular to its velocity vector and with the initial exhaust gas-containing region encompassing the IBSS line of sight as indicated in Fig. 2.

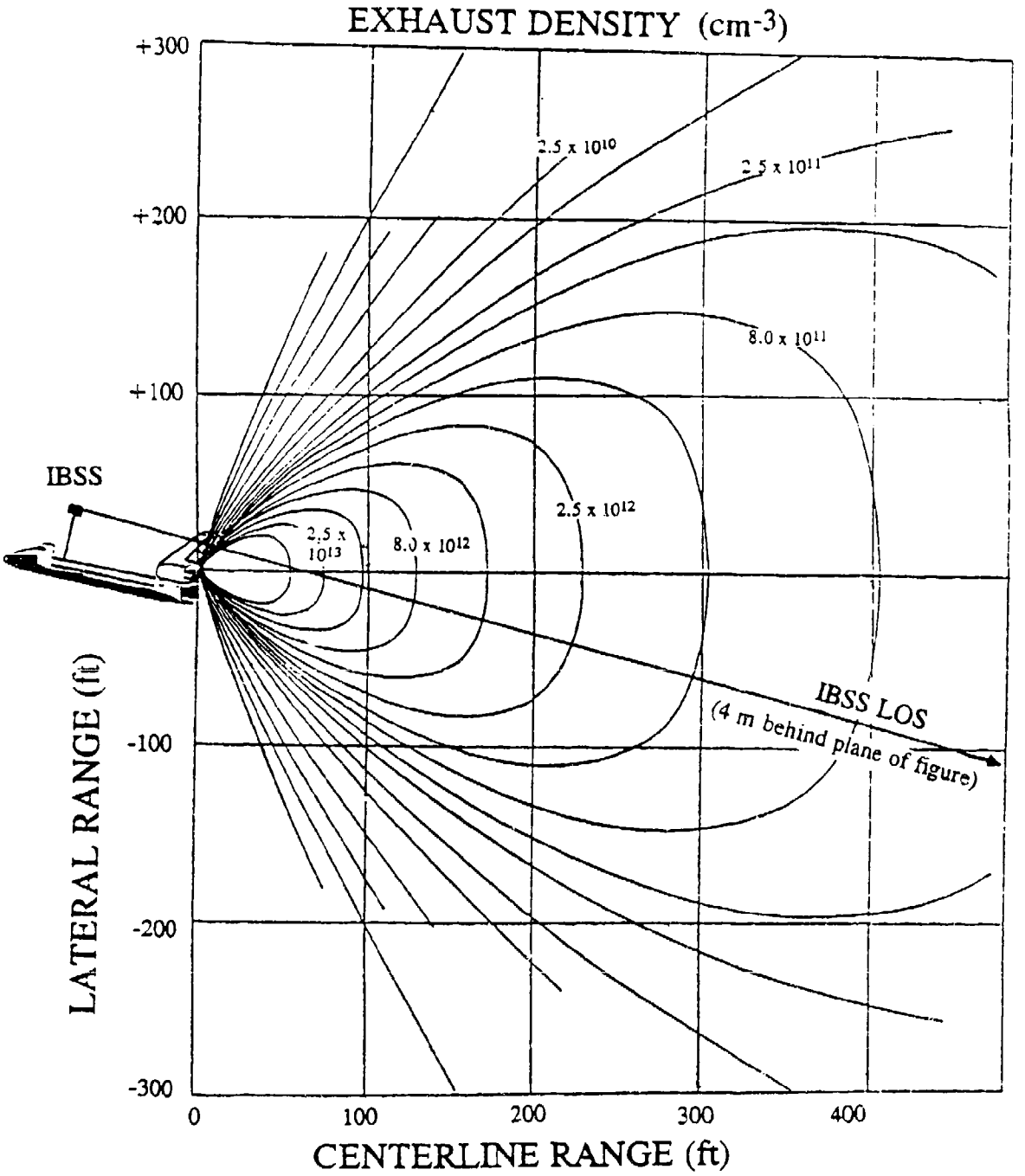

Figure 2. Predicted density contours of combustion-product gas from a PRCS engine in a plane through the symmetry axis (from Ref 8). The IBSS line of sight shown is 4 m behind this plane, an effect taken into account in calculating column densities within its field of view in Fig. 6b. Ambient air density is 3.5×10^9 molecules and atoms/cm^{-3}, substantially less than the exhaust-gas densities at these distances. On this scale the the primary atmosphere-interaction volume would lie roughly 1 m to the right of the page.

The images from the video camera show no particular enhancement of visible "shuttle" glow off the windward side of the vertical stabilizer (*3)* above), but rather a widespread diffuse pattern similar to that appearing in NASA silver halide color images from onboard of PRCS engine firings. In addition the IBSS field of view passes about 5 m beyond, and at least 4 m to starboard of, the ~3 m-long narrow inner visible-radiating region prominent in both spectral images of the close-in exhaust (Ref 6) and in these widely-distributed photographs.

That segments of the "far-field" atmosphere interaction region of L3A (*2)*) are viewed by IBSS is indicated by the aforementioned groundbased video images of a similar engine burn illustrated in Fig. 3 (from Ref 3). Several such PRCS firings perpendicular to space shuttle's orbital track have been photographically observed to produce a few kms-long visible emission pattern weighted toward the ram-directed side of the exhaust stream, and which appears to extend continuously back to the spacecraft body proper. (In contrast wake-directed firings such as L1L show much weaker visible glow, with radiances below the threshold of intensified video cameras from the air volume into which IBSS is pointing (Ref 3).) This would be the region viewed by the spectrometer, whose coaligned video camera indeed shows unstructured visible radiation originating from the starboard side of Orbiter's vertical stabilizer (and weak signal from the port side where the thruster engines are physically located).

However, the vibrational-band and rotational-line radiations to which IBSS responds can not be expected to arise from the same excitative and fuel fragment-involving reaction processes as the more energetic electronic-band and -line photons that video and film cameras see (Ref's 2 - 4). That is, the visible light images do not reliably locate the source of rovibrational excitation and radiation measured by the IR sensor. Additionally, H_2O and CO_2 molecules leaving Shuttle Orbiter's vertical stabilizer in excited states radiate over long pathlengths relative to the size of this potential recombination-stabilizing surface, with the result that the infrared radiances in the IBSS field would be small in comparison with those of the much shorter radiative lifetime visible electronic transitions (as is explained in detail in Ref 7). For example emission near 6.3 μm from the 0.05 s-lifetime 010 vibrational state of H_2O would originate from over roughly (0.05 s) $\times$ (600 m/s desorption velocity) $\approx$ 30 m from the point of excitation, and the much longer-lived rotational states would radiatively depopulate over several 10's km. Even more important, the high rotational and vibrational temperatures that we report below are inconsistent with the ~250K kinetic temperature of Orbiter's outer surfaces. We thus conclude that excitative recombination (process *3)*) makes a small contribution, if any, to the IBSS spectrum data analyzed here.

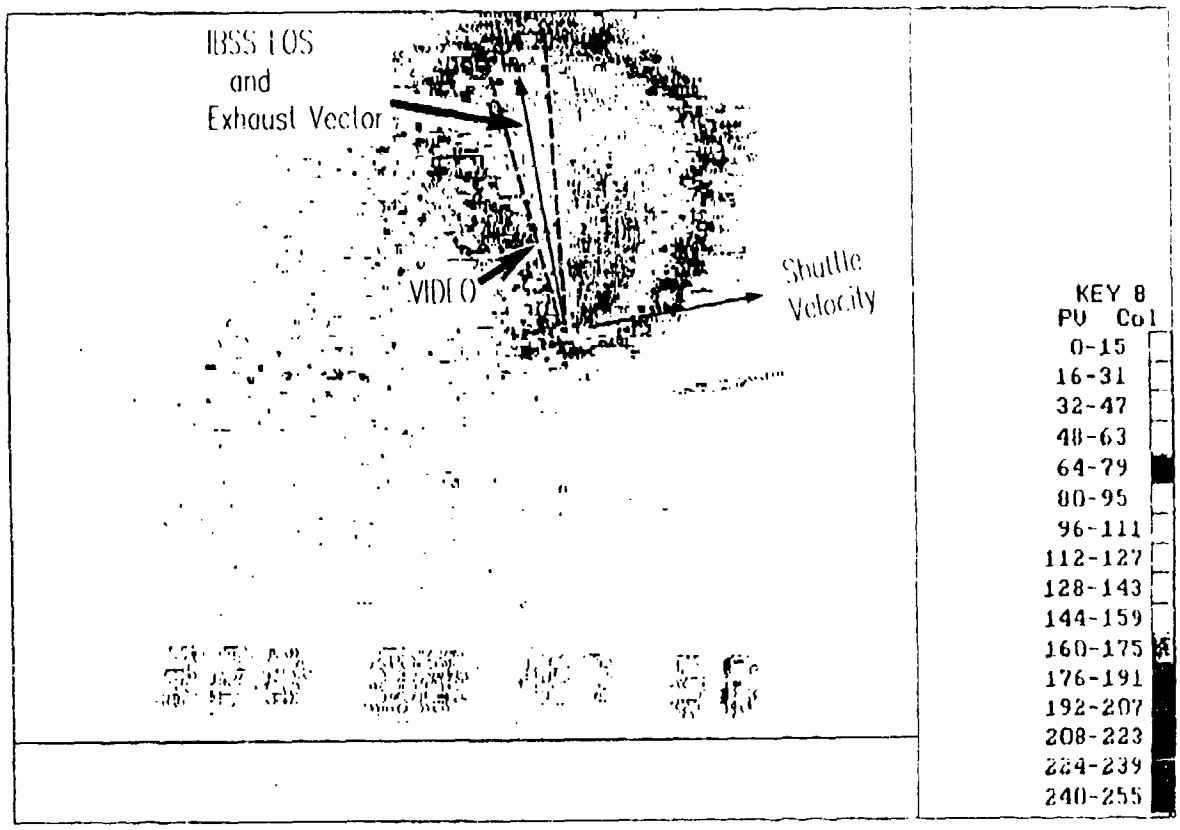

Figure 3. Atmosphere interaction volume of a perpendicular-to-track PRCS exhaust stream near 300 km as imaged by a groundbased visible light-sensitive camera (Ref's 2, 3). The exhaust axis and IBSS line of sight vectors are directed -57° out of the image plane (towards the viewer). Diagonal field of view at Shuttle Orbiter's range is 5.6 km.

Table 1. Characteristics of a shuttle PRCS engine and its exhaust gas.

Mass Flow Rate (g s^{-1})	1419.8
Exhaust Velocity (km s^{-1})	3.5
Chamber Temperature (K)	3038
Specific Heat Ratio of Exhaust	1.292
Thrust (lbs)	870.0
Effective Nozzle Expansion Angle (°)	21.77
Solid-Phase Limiting Streamline Angle (°)	53.37
Farfield Contaminant Fraction	0.03

The single projection to an onboard camera does not directly identify the infrared emissions as originating from within volumes *1)* or *2)*. However, the short rise times (~1/20 s) of the spectral signal at engine turn-on (see for example Fig. 7 at 16.6 μm or Fig. 9 at 7.3 μm) imply that the primary emission source is within the "near field" shown in Fig. 2, as the transit time of combustion molecules to volumes where they collide principally with atmospheric species is of order 1/3 s. In either case--"thermal" radiation from the exhaust gases, or their re-excitation by high translational energy collisions with the atmosphere--a logical initial analysis procedure is to characterize the spectral distributions by single Boltzmann temperatures. In consequence we first consider the emission as due to "thermal" population, in exhaust gas whose density substantially exceeds that of the ambient atmosphere (as is for example shown by Fig. 2*)*. This standard equilibrium-thermodynamics approach turns out to produce reasonably internally consistent results.

PRCS - Exhaust Properties

The performance characteristics of the liquid-bipropellant PRCS engines in Table 1 are based on the CONTAM III model (Ref 8). Kinetic temperature at the exhaust exit plane is calculated as 3000K, and the initial directed velocity of the thrust-producing gas stream is 3.5 km/s. In addition to the primary combustion product molecules H_2O, N_2, H_2, CO, and CO_2 (in order of abundance), secondary species including O_2, OH, NO (the oxidizer is N_2O_4) and also very roughly 1-3% mole fractions of highly-reactive unconsumed fuel (monomethyl hydrazine) and its incompletely-burned molecular fragments (such as C_2H_2, Ref 6) are expected. The readily-excited H_2O vibration-rotation bands and the CO_2 ν_2 and ν_3 sequences have been observed previously to be among the principal emissions from the region near similar thruster engines. These excited vibrational states have lifetimes of 10^{-2} - 10^{-1} s, and those of the pure rotational states of H_2O are on the order of 10 - 100 s.

Exhaust Flow

Several paired PRCS engine firings took place during the ~2-min experiment period (0017 - 0019 UT), each approximately 0.5 s in duration. In most of the burns the two engines pulse alternately each 0.04 s. As this cycle period is comparable with the transit times through the IBSS field and radiative lifetimes of the combustion-product species, this discontinuous input of exhaust gases does not appear to be affecting the spectral intensities. However the infrared emission data can be considered as referring to transient behavior, before and after "equilibrium" is established in the PRCS engine chamber and (in particular) the atmospheric-interaction volume (Ref 3). The effect can be seen in the onboard video images, which show excess scene brightnesses just after engines turn on.

These routine control engine burns, whose precise timing was provided by NASA, are uncorrelated with the continuous sequential wavelength scans of IBSS, whose timing is reported to within 1 s. Nonetheless the actual positions in the spectra at which firings started and stopped are in general identifiable from the relatively rapid increases or decreases in spectral intensity. In isolated cases incomplete coverage of the full rotational development of an individual vibrational band, or of a sequence of bands, hampers spectral identification and/or assignment of a "temperature".

The volume densities of gas exhausted from a single PRCS firing into vacuum in Fig. 2 refer to a plane through the longitudinal symmetry axis of the rocket motor. The actual IBSS line of sight misses these contours by several m in the Y direction (i.e., it is behind the plane of the figure), with the result that the column densities in its field of view are somewhat lower than those suggested by the two-dimensional plot. We took this effect into account in calculating the column densities in later Fig. 6. Density and kinetic temperature both decrease rapidly as the exhaust gas expands adiabatically, as replotted in Fig. 4. The geometric-collision rate (Fig. 5) is falling correspondingly rapidly, and by 15 m from the engine exit plane has become less than the lowest radiative decay rate of the excited vibrational states mentioned above. We combined the collisional deactivation probability of these states (from the standard journal literature) with this elastic collision rate to determine the downstream distance at which radiative decay of the molecules "decouples" from their quenching/excitation. Table 2 lists these probabilities along with transition rates and estimates of column densities in excited states densities based on thermal equilibrium in the canonical exhaust volume shown in Fig. 2. We return to this critical issue in the data analysis below.

Table 2. Calculation of excited state densities based on absolute band radiances and known transition probabilities.

	Ground state column density [10^{15} molecules/cm^2]	Band radiance from IBSS [W/cm^2-ster-μm]	FWHM [μm]	Decay rate [s^{-1}]	Excited state column density [10^{13} molecules /cm^2]
CO_2(010)	5.0	1.3×10^{-6}	0.075	1.6	4.4
H_2O(010)	41	2.0×10^{-6}	~1.0*	19.9	4.0
H_2O(J=12)	41	2.0×10^{-7}	0.1	~0.01	210

* The complete H_2O(010) rovibrational band was not measured; total band is estimated.
J Refers to rotational state.

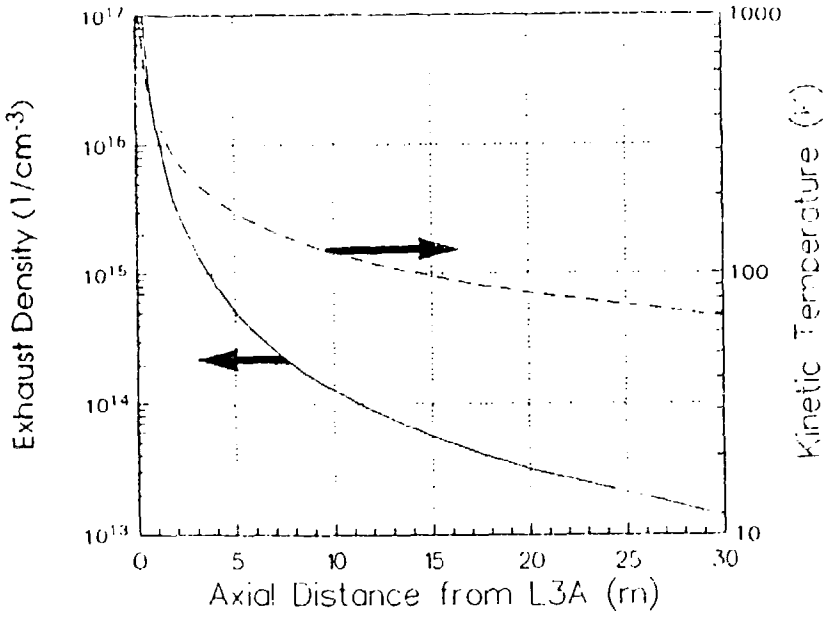

Figure 4. PRCS exhaust gas density and kinetic temperature as a function of distance along the thrust vector. Adiabatic expansion with $\gamma = 1.29$ was assumed for extrapolation toward the engine exit plane from the CONTAM model results.

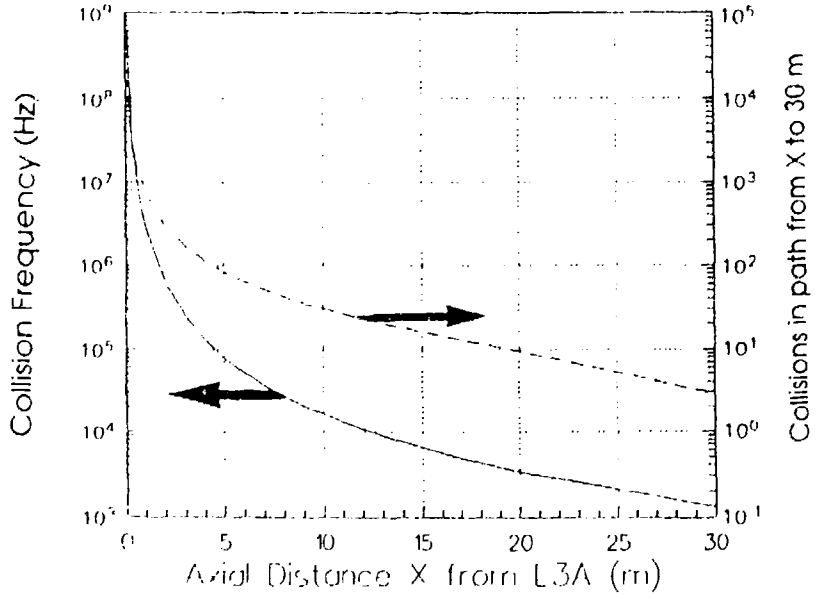

Figure 5. Elastic-collision frequency (based on the densities and temperatures of Fig. 4) along the thrust vector, and number of collisions of individual molecules as they travel from a starting point on the exhaust axis (X) out to 30 m from the engine exit plane. A mean collision cross-section of 4×10^{-15} cm^2 is assumed.

Spectra

The wavelength-scanning spectrometer operated continuously, covering 2.5 to 24 μm in first order in 16 s, while the short-duration PRCS firings to maintain Orbiter's aspect along its relatively low altitude trajectory took place sporadically with an average separation near 15 s. The individual segments recorded by IBSS were typically 0.7 μm in spectral width. (The twelve detector elements in its image plane are divided into six pairs each covering a separate spectrum band, with the photocurrents recorded in parallel; many of the spectra were in other than first order.) Overall approximately 30 small spectral segments, postprocessed with absolute radiometric calibration under the direction of Phillips Laboratory, were made available for this analysis.

The stated resolution of the Ebert-Fastie design IBSS spectrometer is 300. We measured base-to-base linewidths of 0.063 and 0.031 μm at 17.2 and 7.45 μm respectively (on isolated rotational lines), which implies a figure nearer 250. We applied this triangular system response in compiling synthetic spectra for comparison with the data as described below. These spectra were found to best fit the measured emission spectra when they were shifted relative to one another by small (constant over narrow ranges) wavelength increments; the largest such displacement is -0.08 μm, to the 16 - 18 μm IBSS data, and the other spectrometer channels called for shifts of order 0.02 μm in no single direction and also without detectable evidence of nonlinearity of their as-presented wavelength scales. Since the fits of wavelengths so reinterpreted then become very close over broad spectral ranges, the observed offset is more likely due to systematic miscalibrations of the instrument or some slip in electronically processing its spectra for distribution than to systematic error in (or application of) the band and line model described just below.

Data Analysis Methods

We pieced together the short wavelength segments from separate engine burns to produce contiguous sections wide enough for coherent analysis (for example, containing, complete rovibrational bands). The wavelengths, with identifying letters to key to the analysis are shown below. Figures 7 - 12 present the IBSS data, and a summary of our findings for this less than fully-covered spectrum region appears in Fig. 13.

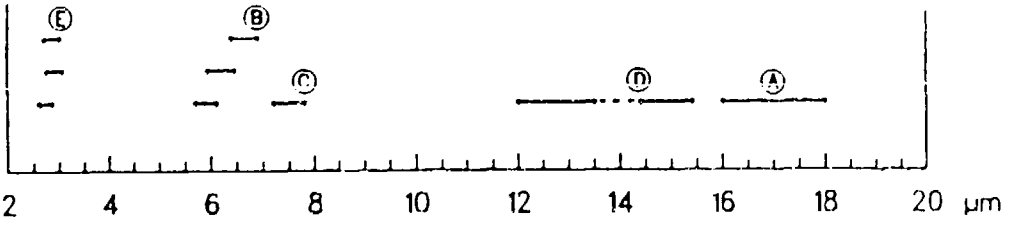

The primary approach applied was comparison with synthetic emission spectra calculated by the HITRAN atmospheric-radiance and -transmission model (Ref 9). This highly-developed simulation code assumes thermodynamic (but not chemical-composition) equilibrium in, and emission from, local gas volumes; it takes into account reabsorption (optical thickness) effects, but makes no provision for physical transport from the regions in which excitation takes place. The upper and lower vibrational states of each transition in the HITRAN database are accessible, but no indication of rotational quantum numbers is given. As HITRAN is designed primarily for application to the always < 1200K earth's atmosphere it is subject to loss of accuracy at higher temperatures; nonetheless its predictions are reliable at lower temperatures, and furthermore the simulation is programmed for convenient application to volumes containing CO_2, H_2O, and other neutral gases common to the natural atmosphere and the exhaust (or further reaction products) of liquid-bipropellant rocket engines. Virtually all other models of infrared radiation from heated gases have the same weaknesses as HITRAN, forcing Boltzmann population distributions and providing no mechanism for the movement of excited species into and out of sensor fields.

We applied HITRAN to determine best-fit single temperatures for the exhaust volume viewed by IBSS over each of the limited spectrum ranges. Although this is a very basic approach to modeling an obviously complex scene, as already noted it does create a reasonably accurate description of the infrared spectral radiances along the line of sight by a limited number of parameters (temperature and column density of radiating species). That is, the HITRAN-based method turned out to provide self-consistent results despite the fact that thermodynamic equilibrium cannot be expected to obtain in either the close-in expanding exhaust gas or the volume in which it reacts chemically with the atmosphere (and that all the gas within the IBSS field of view would not be at a single "temperature").

We also applied a second analytical approach to interpreting the spectra based on the decay rates from molecules in the observed vibrational states. This involved deriving absolute column densities of excited molecules from the measured absolute spectral radiances and known transition probabilities. (While only the first vibrational level was considered, populations in higher levels can be estimated by taking into account cascade with the appropriate branching ratios.) The total column-concentrations of exhaust species within the IBSS field were determined from the CONTAM total-density contours in Fig. 2. This line of sight is not accurately plotted as a straight line on this contour maps but actually follows a hyperbola, as is plotted in Fig. 6; integration along this path provides the total column density of exhaust in all excitation states. Applying the known 0.328 and 0.036 mole fractions of H_2O and CO_2 from PRCS engines, their column densities within the IBSS field were calculated to be 4.1×10^{16} molecules cm^{-2} and 4.5×10^{15} molecules cm^{-2} respectively.

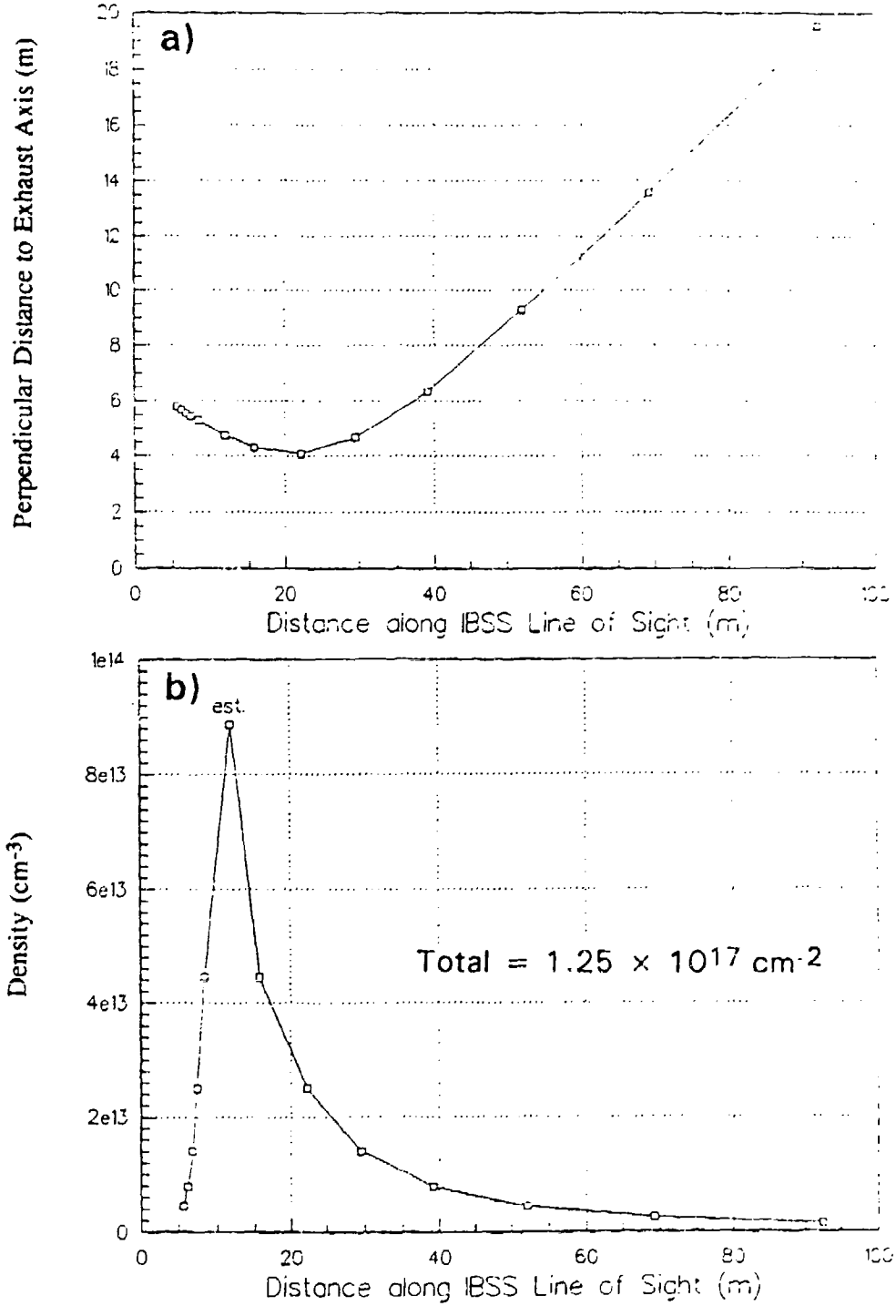

Figure 6. a) Path of the IBSS line of sight (skew to the exhaust axis), which describes a hyperbola in a rotating plane containing the axis. Its closest approach to the exhaust axis, 4 m, occurs at approximately 20 m downstream from the exit plane. b) Exhaust density along this line of sight, and integrated to provide a total column depth.

The results of comparisons with HITRAN predictions immediately below, which as noted fit the distributions in excited states with single (thermal-equilibrium) temperatures, are presented in the order of our confidence in this analysis and its spectral identifications to date.

HITRAN Spectrum Analyses

LWIR (A in the diagram above; refer to Fig. 7)

This ~16 - 18 μm data set shows primarily pure rotational emission from H_2O. The absolute radiances at wavelengths between 16.6 and 17.4 μm (with the exception of the segment 16.8 to 17.0 μm) and application of the above-stated number of water molecules in the sensor field give a good fit to 800K as the effective rotational temperature; the 1200K HITRAN prediction also fits the relative, but not the absolute, line intensities. Lack of agreement below 16.6 μm and above 17.4 μm is interpreted as due to the thrusters not firing during these sections of the IBSS scan.

Some of this 16.8 to 17.0 μm difference can be made up by addition of a column of CO_2 with the 1/10 density of H_2O predicted by the exhaust composition model and the same rotational mode-equilibrated temperature; see Fig. 7b. After subtraction of the HITRAN synthetic spectrum from the wavelength-corrected IBSS spectrum (Fig. 7d) the remainder is a feature centered at just below 16.9 μm, which we judge to be the CO_2 (030 $^1\Pi_u$ - 020 $^1\Delta_g$) "hot" fundamental band not included in the HITRAN database.

5.7 - 6.9 μm (B; Fig. 8)

Data from the three overlapping spectrometer channels indicated in the diagram above were pieced together to produce the plot in Fig. 8a. The signal is due almost exclusively to the readily-excited H_2O ν_2 (bending mode) vibration-rotation transitions. Tests at several other temperatures (not shown) show that these data best fit an 800K ($\pm$400K) HITRAN synthetic spectrum.

The discrepancy at wavelengths between 6.1 and 6.3 μm was again addressed by subtracting the measured and synthetic spectral distributions, with the result shown in Fig. 8b. (The amplitudes were not normalized to one another.) The broad difference feature makes a seemingly plausible visual fit to the NO_2 ν_3 rovibrational band at 400K. This match is definitely not unique, as a non-Boltzmann distribution of excited states of H_2O could also account for this relatively low signal/noise feature. Indeed, the positions in the HITRAN prediction of all four local maxima between 6.1 and 6.3 μm agree with those of the measured spectrum; only the amplitudes fail to match up.

Furthermore, NO_2 is calculated by rocket engine performance models to be present in PRCS exhaust only at very low concentrations. The column density of NO_2 in the IBSS field

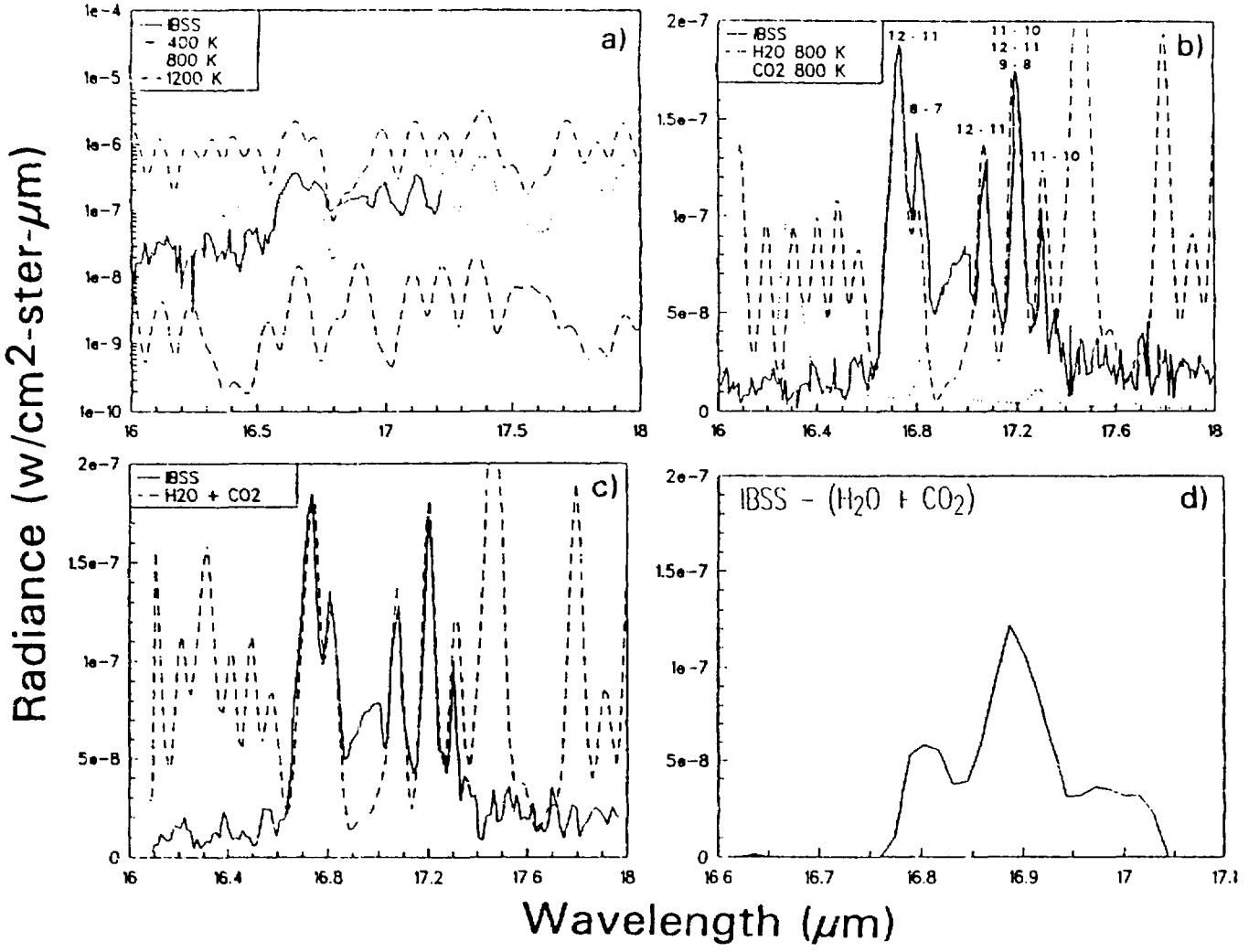

Figure 7. a) Absolute comparison between IBSS and synthetic HITRAN spectra of a column of H_2O in thermal equilibrium at three different temperatures. b) Specific H_2O pure rotational lines identified and predicted CO_2 spectra. c) Sum of H_2O and CO_2 synthetic spectra compared with IBSS data. d) Remainder after subtraction of the synthetic spectrum. (IBSS spectra in this wavelength range were shifted by -0.08 μm to match the synthetic spectrum.)

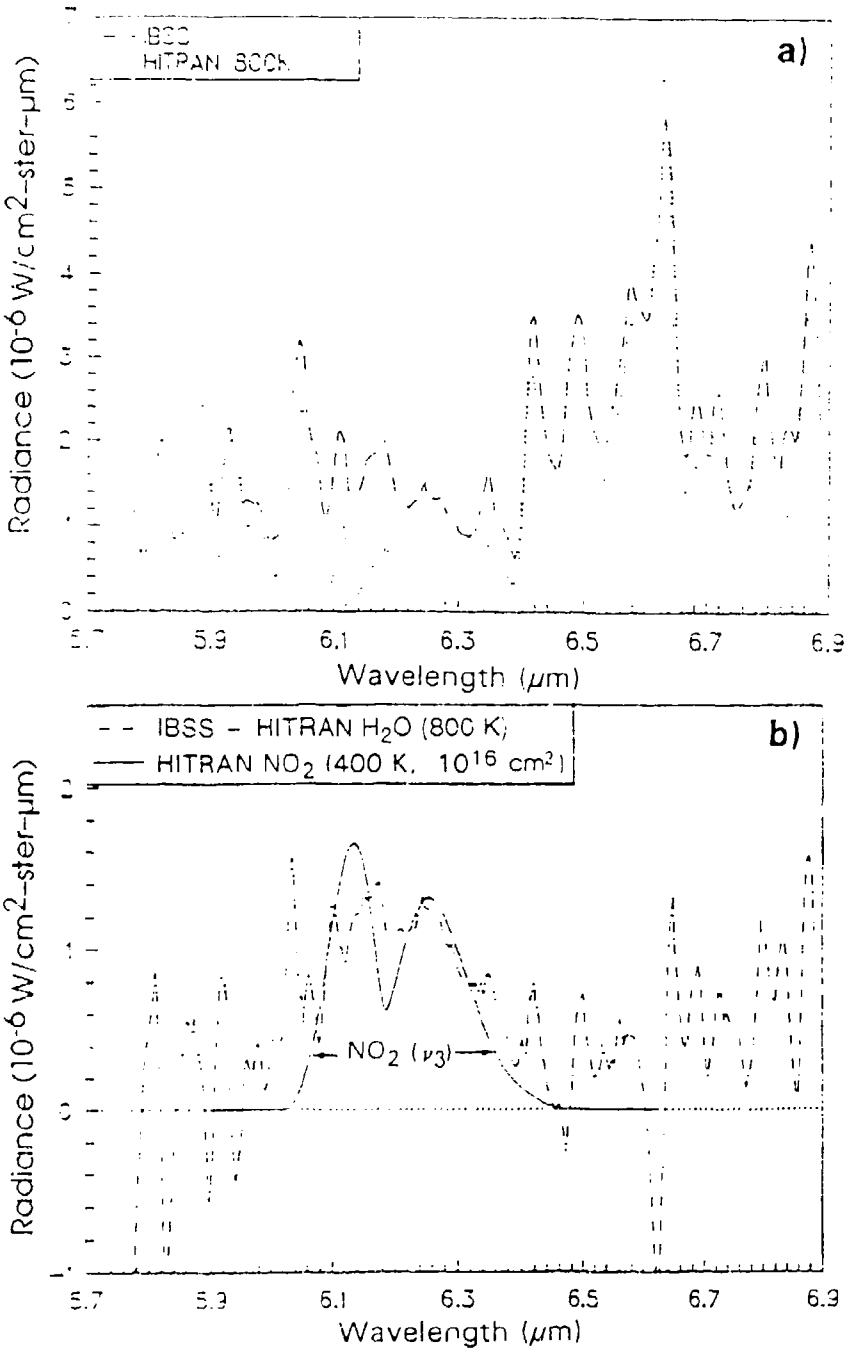

Figure 8. Three segments of IBSS exhaust spectrum joined together a) compared with the best-fit synthetic spectrum and b) differenced to identify a feature near 6.2 μm. (Noise in the subtracted spectrum is believed due to a somewhat incorrect wavelength shift of the data before subtraction.)

needed to fit the amplitude of the 400K spectrum is 1×10^{16} molecules cm^{-2}, which is as high as that of CO_2 and substantially greater than predicted by CONTAM. Still further, if the process exciting the infrared emission were vibrational cascade following electronic excitation of NO_2 molecules by recombination of exhaust NO with ambient or exhaust O, the measured infrared column intensity of 10^{14} photons/cm^2 s would lead to visible quasi-continuum emission of about this considerable magnitude (which is 100 megarayleighs). No such strong visible glow has ever been observed in rocket exhaust investigations, and furthermore the plausible upper limit to the rate of such reactions is far less than would be required to result in the measured infrared radiance. We interpret the difference feature as due primarily to out-of-thermal equilibrium excitation of water vapor in the exhaust.

7.2 - 8 μm (C; Fig. 9)

Here H_2O is again clearly identifiable as the principal radiating species, with 1200K giving the best fit to the spectral distribution. After subtraction of fractions of the water synthetic spectra from the measurements, maintaining the predicted 1:10 ratio of CO_2 to H_2O molecule concentrations (Fig. 9b), the hot bands of CO_2 known to exist throughout this spectrum region leave the impression of being present. However the data on the intensities of these features must be regarded as still inconclusive.

Near 15 μm (D; Fig's. 10 and 11)

Approaching the very strong CO_2 ν_2 fundamental band from the short-wavelength side (Fig. 10), the fit of HITRAN is poor because its database does not include several transitions from high-lying vibrational levels of CO_2. Nonetheless the general trend is as expected.

Closer to 15 μm (Fig. 11) the fit improves greatly, and a temperature assignment of at least 800K can be made based on the multiple-band structure near 14.5 μm. Water rotation bands are definitely interspersed here, as is expected from LWIR spectrum A. Broadening of the 15 μm ν_2 feature is due to the $2 \rightarrow 1$, $3 \rightarrow 2$,... vibrational transitions rather than to rotation, as evidenced by fits to it (not shown).

SWIR (E; Fig. 12)

The short wavelength region (still under investigation) shows the expected H_2O ν_1 and ν_3 fundamentals near 2.7 μm and hybrid bands of CO_2 terminating on the ground state (021 - 000 and 101 - 000). While the line positions fit reasonably well, no unique excitation temperature emerges. Some of the structure might be attributable to OH fundamental radiation (note for example that the strong Q branch of the 1,0 band at 2.81 μm aligns with a spectrum peak). No evidence of the NO vibrational overtone is present.

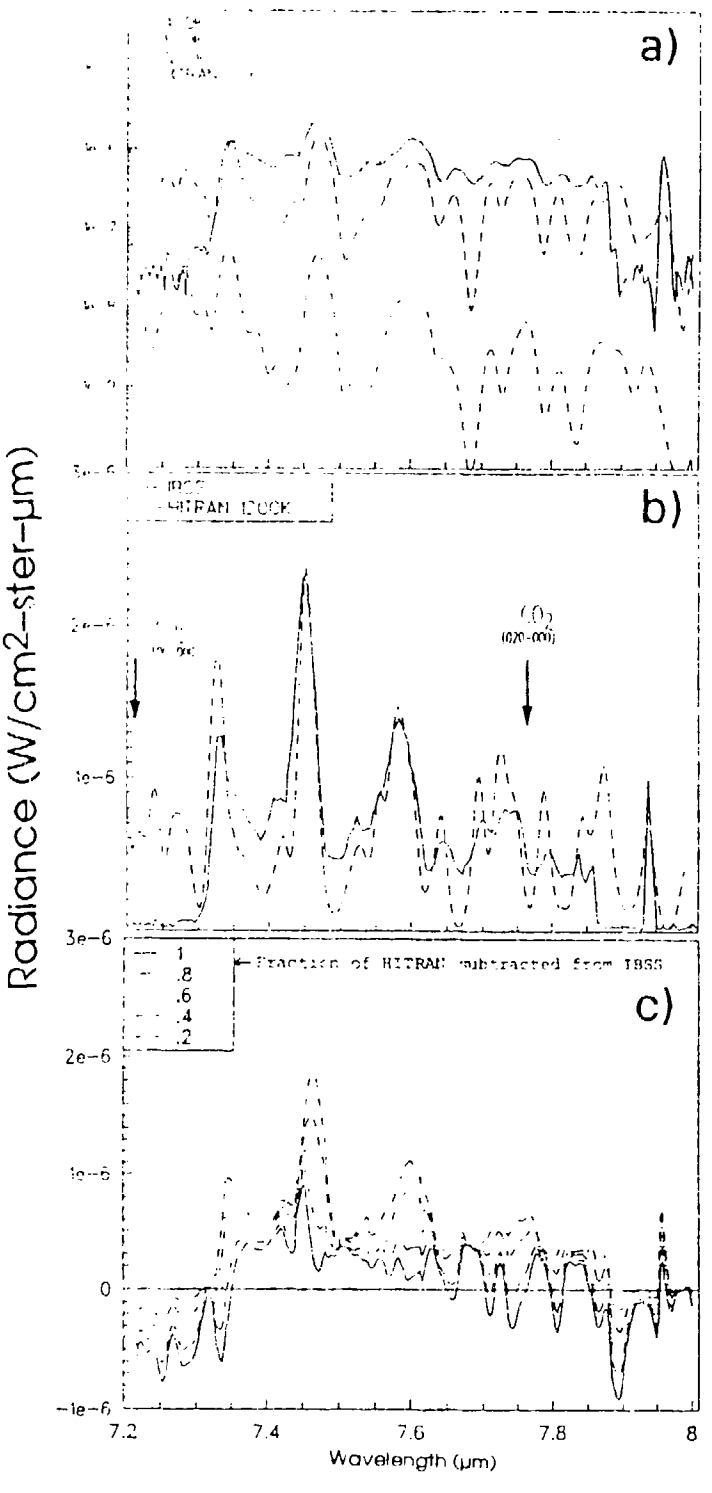

Figure 9. a) Plots showing that the best fit of the portion of this spectrum segment to HITRAN is with a 1200K excitation temperature. The principal feature is the P branch of H_2O 0.0 - 000. b) Comparison of IBSS to 1200K HITRAN on a linear scale. c) Result of subtracting fractions (or all) of the best-fit spectrum from the IBSS radiances. (The IBSS spectrum has been shifted by +0.06 μm.)

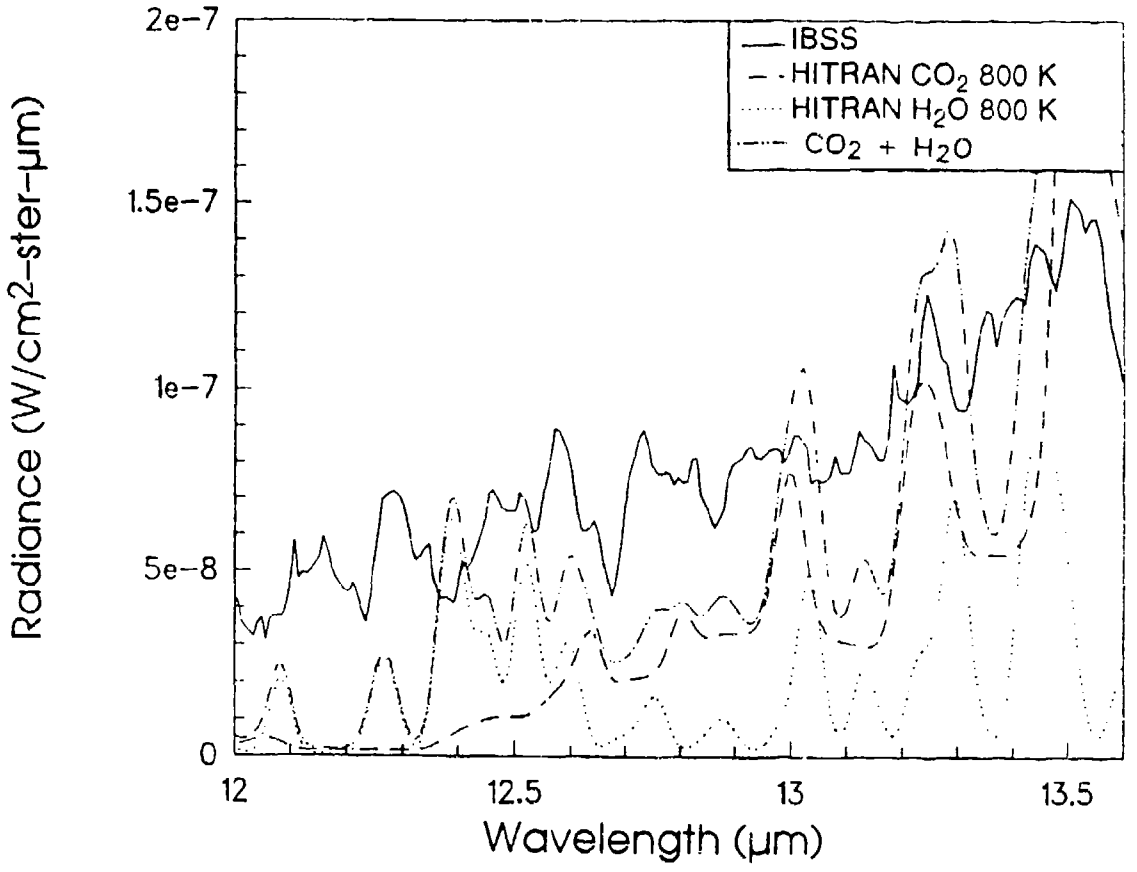

Figure 10. Comparison of the general trend in the spectral region below the CO_2 ν_2 band at 15 μm. No specific match of structure is apparent.

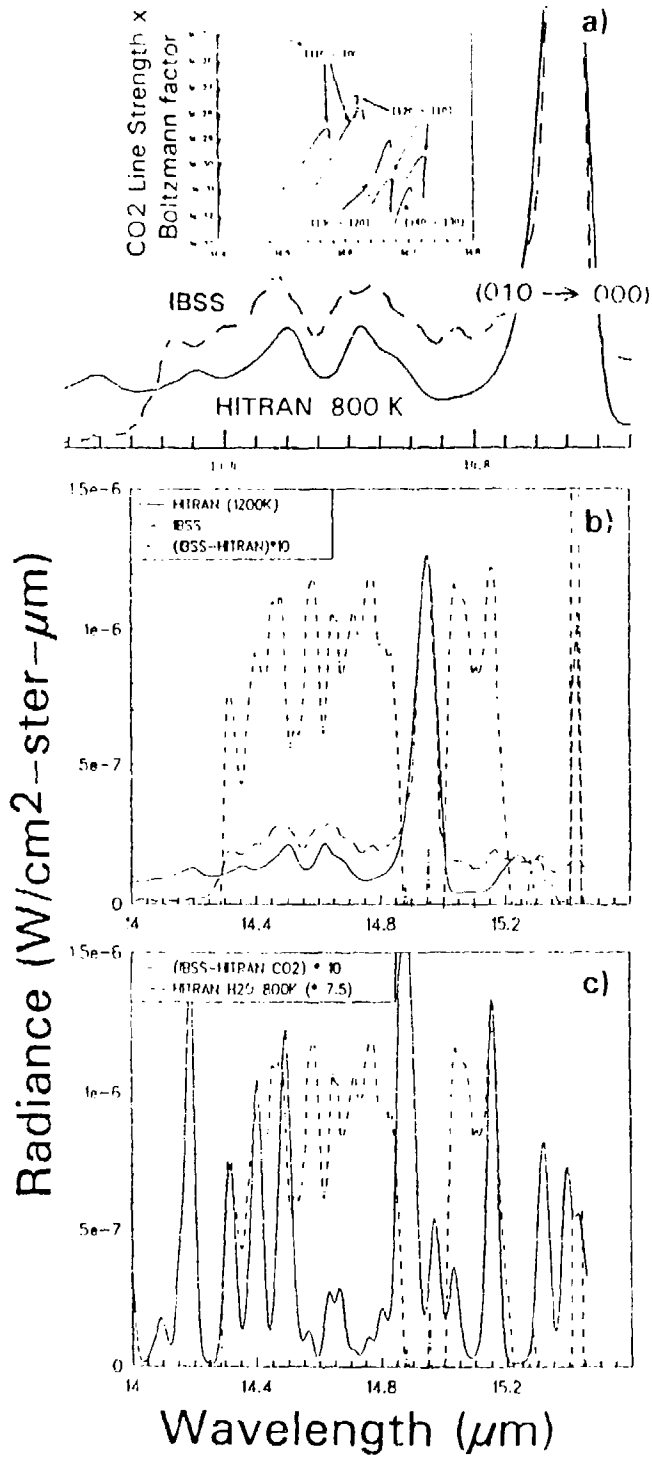

Figure 11. a) LWIR segment showing the strongest feature of all the IBSS spectra to be the CO_2 ν_2 fundamental broadened by hot bands (to its short-wavelength side), and displaying many hybrid bands (also toward short wavelengths). b) Subtraction of the 1200K CO_2 model spectrum, which reveals an underlying H_2O rotational spectrum. c) Fit to 800K H_2O in this region.

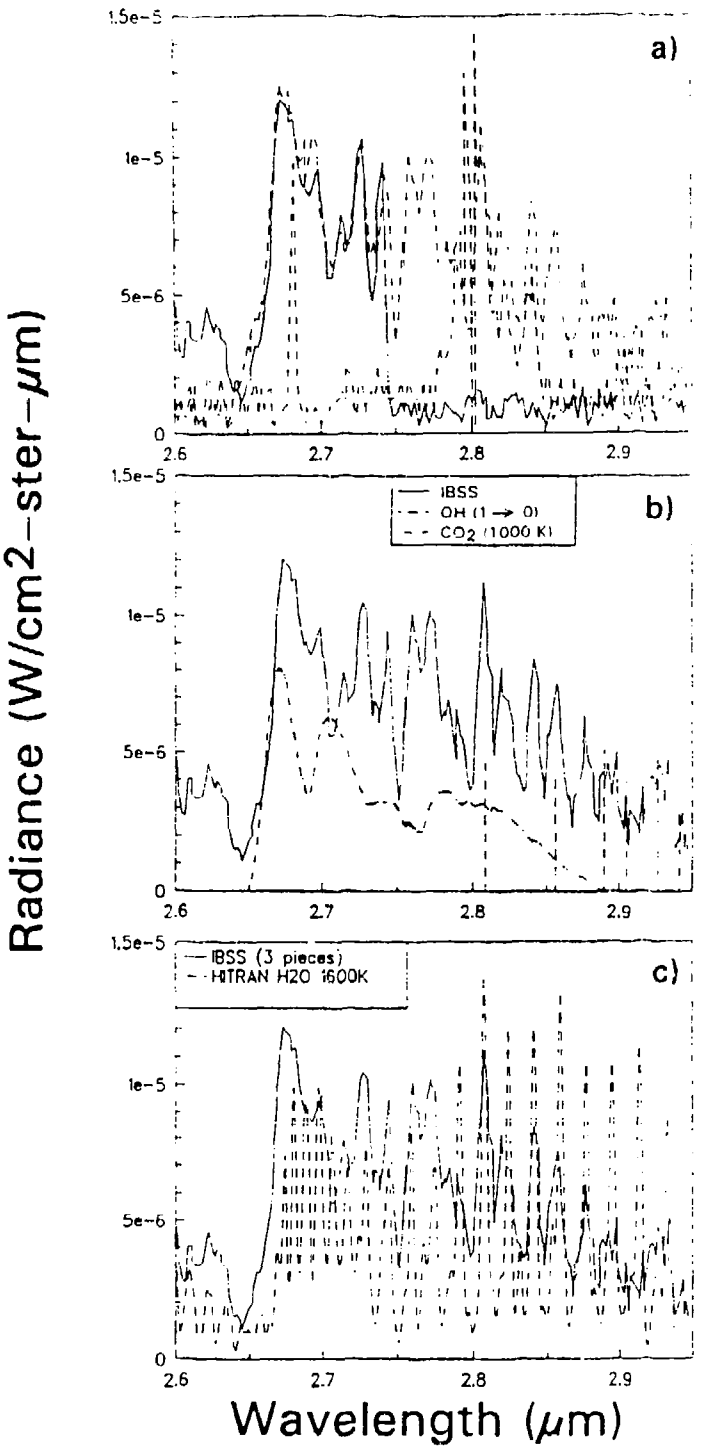

Figure 12. a) Three single segments of SWIR data. b) The three segments combined to form a contiguous section from 2.65 to 2.95 μm, with a synthetic spectrum of CO_2 and OH lines (refer to the text). c) A rotationally-hot (1600K) H_2O ν_1 and ν_3 synthetic spectrum fits some of the measured structure.

Calculation of Densities in Excited States

While the spectral distributions in Fig's. 7 - 12 are reasonably self-consistently describable by a unique radiation temperature, the fractions of H_2O and CO_2 molecules in upper vibrational states are by and large less (relative to the totals from CONTAM in Fig's. 2 and 4) than predicted by equilibrium thermodynamics for this temperature. If the emissions measured by IBSS originate primarily in the expanding exhaust-gas volume of Fig. 2 (*1*)--rather than in the more widespread and much lower collision-frequency atmospheric-interaction region of Fig. 3 (*2*)--this may be due to transport of internally excited molecules into the IBSS field. As can be seen, this field intercepts the projection of the exhaust axis several m away from the engine exit plane, and in fact contains gas at a wide range of predicted temperatures. We therefore considered the potential effect of collision-limited radiation along the gas-expansion and -cooling path of the upper states of three of the principal infrared emission features, as summarized in Tables 2 and 3.

Approximately one of every 250 gas-kinetic collisions of ~800K CO_2 with H_2O quenches the (010) excited state of CO_2, and the H_2O (010) state is some 30 times more probably depopulated (or the excitation transferred) in collisions with ground vibrational-state H_2O molecules. Rotationally excited H_2O in contrast very efficiently transfers its energy to/from translational energy. Thus rotational temperatures decrease in the expansion about as rapidly as kinetic temperatures, while the less probable (per collision) depopulation of vibrationally excited states leads to the internal "temperature" of the molecules--CO_2 in particular--decoupling from the kinetic temperature of the gas at its higher temperatures further upstream; that is, the distribution in vibrational states becomes "frozen in" nearer the engine exhaust plane.

Table 3. Comparison of thermal-excitation with measured excitation fractions and number of collisions required to quench the 800K thermal distribution.

	Wavelength [μm]	Energy (upper level) [cm^{-1}]	800K fraction excited	IBSS fraction excited (from Table 2)	Collision deactivation probability (~800K)	Coll's required 800K to IBSS	Inferred temp from IBSS absolute radiance [K]
CO_2(010)	15.0	667	0.21	0.009	0.005*	630	165
H_2O(010)	6.2	1595	0.054	0.001	0.15	25	340
H_2O(J=12)	16.7	2124	0.011	0.05	0.5□	-	3000§

*Based on the CO_2(001) state.

□Estimate based on known rapid thermalization.

§Probably a cascade effect (all higher J levels pass through J=12)

Figure 5 shows the relevant collision parameters in the close-in exhaust volume. The number of collisions suffered by each molecule as it travels from distance X from the exit plane out to 30 meters--beyond where collision rates fall below rates of depopulation by radiation--is based on the CONTAM model local density and temperature in Fig's. 2 and 4, with a temperature-independent cross-section of 4×10^{-15} cm^2 adopted. For example of the $CO_2(010)$ molecules populated according to local thermodynamic equilibrium within the volume close in to the engine, less than 5% would be expected to remain in this state 15 m downstream.

A local column temperature can be inferred from the measured excited state densities by the usual procedure of assuming a Boltzmann distribution. As shown in the last column of Table 3, these temperatures, 165K for CO_2 and 340K for H_2O, are very much lower than the 800 - 1200K temperatures found from fitting the measured spectral structure to HITRAN-generated synthetic spectra. This indicates that the distributions within excited states, weighted over the IBSS field of view, are non-statistical.

Rotationally excited H_2O was also similarly analyzed, by addressing a spectrally-isolated line in the 16.6 - 17.4 μm segment that corresponds to the pure rotational transition from quantum number J=12 to J=11. Although the absolute radiance and spectral width in this sequence fit a temperature near 800K, the measured column density of the upper state (5% of the total H_2O) would lead to a population temperature in excess of 3000K (see Table 3). We judge this large discrepancy is due to cascading from higher rotational states in the out-of-equilibrium volumes, so that a more detailed analysis approach is needed for rotational transitions.

The analyses summarized in Table 3 are as noted based on the column densities within the IBSS line of sight of the ground state-molecules, which we have calculated from the CONTAM symmetry-plane contour predictions with the view geometry corrected as described above. We avoided use of this perhaps-questionable absolute total column concentration by comparing the densities in the $H_2O(010)$ (1595 cm^{-1} above the ground state) and $CO_2(010)$ (667 cm^{-1}) upper levels derived from the measured absolute spectral radiances and Einstein coefficients for the transitions to the ground vibrational states of the two molecules. The ratio of these two upper-level densities within the IBSS field of view would be produced by a Boltzmann vibrational distribution at 420K for both species. This figure is closer to the 800K - 1200K figure that we derived from HITRAN synthetic spectra, but nonetheless it remains indicative of the internal inconsistency that may result from adoption of a model of one-temperature statistical excitation throughout the spectrometer's field of view through the expanding-and-interacting rocket exhaust gas.

Conclusions from the HITRAN-Based Data Analysis

Figure 13 summarizes the infrared spectrum regions investigated, and identifies the principal emission features that would contaminate onboard optical remote sensing or surveillance in the particular oblique field of view of IBSS during ~½ s-duration liquid-bipropellant engine firings. Attention is directed to the fact that several wavelength regions that may contain further radiations are not represented in these data (in particular 4 - 5 μm, where the CO_2 ν_3 and CO fundamental vibration bands appear); and that the sensor line of sight includes both rapidly-expanding exhaust (but still denser than the local atmosphere) and more distant volumes in which this high translational-energy gas experiences inelastic collisions primarily with air species (for example H_2O + O producing H_2O (010 and 001); see Ref 5). The intensities and temperatures of the emission give strong evidence that it is a "volume" effect rather than resulting from spacecraft surface-assisted processes, and the rapid ($\lesssim$1/20 s) rise times show that most (perhaps all) of the emission is arising from within ~200 m of the PRCS engine exhaust plane.

The primary results of comparisons with synthetic spectra are as follows.

1) Without question the principal radiating species within this IBSS field are H_2O and CO_2. Their expected (complex) vibrational features are present at high signal/noise, and most of the remaining spectrum maxima can be interpreted as due to either non-Boltzmann populations of upper states of these molecules or omission of high-lying transitions from the referencing predictive model. No other species, or continuums from thermally-radiating particulate exhaust, can be considered as identified so far. As noted the incomplete spectral range analyzed does not include several fundamental vibrational bands of molecules whose electronic bands have been identified in various regions of PRCS exhaust, including CO and NH and CH; furthermore the HITRAN spectrum simulation omits ion species, notably H_2O^+ (its strong bands are near 3 and 7 μm), which are expected to be vibrationally excited by the fast charge-exchange collisions (Ref 10) with the O^+ abundant in the ionosphere.

2) The relative and absolute spectral intensities give evidence of an effective radiation "temperature" of 800 - 1200K, and possibly higher. The absolute radiances are in general less than those that would result from the column-concentrations of exhaust species in the near field predicted by CONTAM, indicating that much of the vibrational excitation is "frozen-in". This average single temperature is an appropriate parameter for defining the infrared signature at the IBSS intercepts on the PRCS exhaust flowfield for the purpose of characterizing optical contamination in Orbiter's environment, rather than an actual thermal-equilibrium temperature of either the combustion products or of these gases when they are re-excited by collisions with the orbital atmosphere.

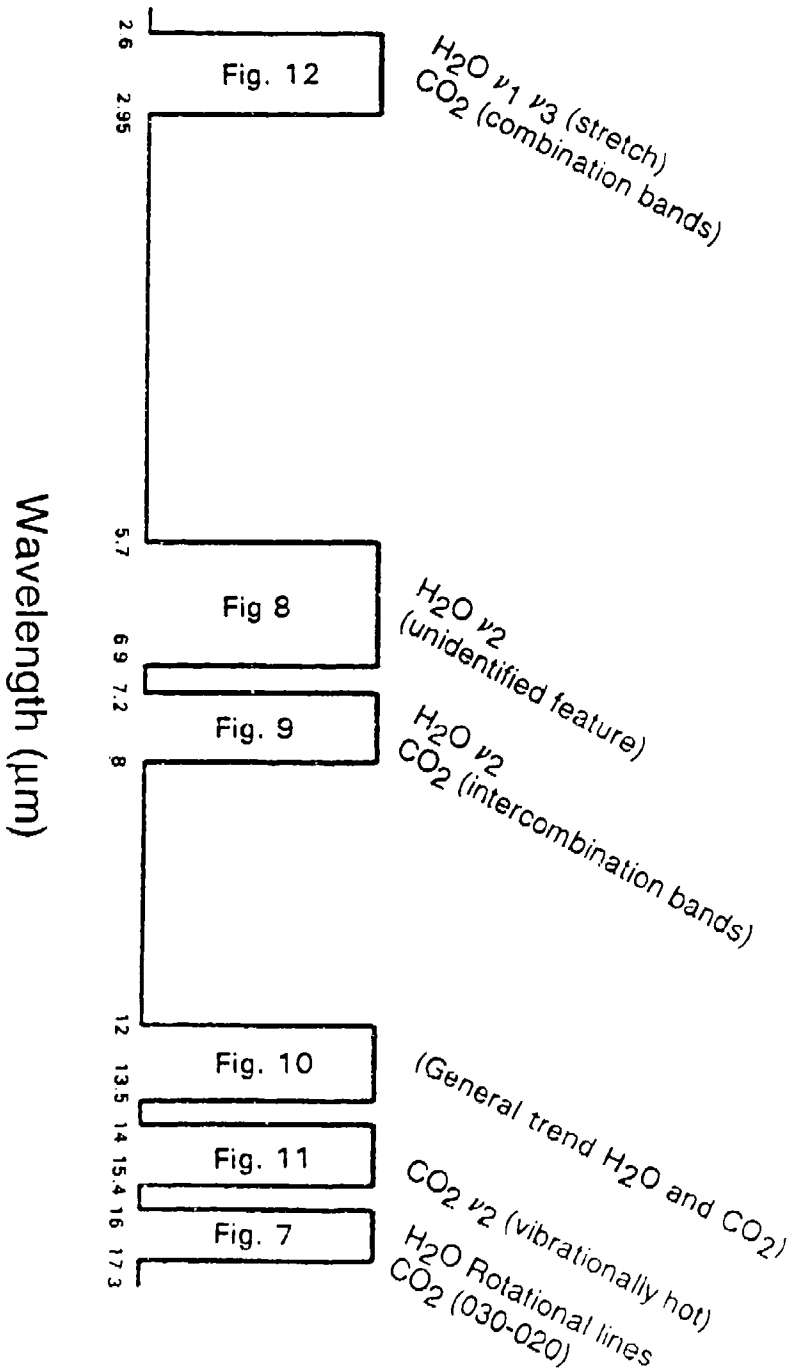

Figure 13. Summary of infrared spectrum regions covered by the IBSS Orbiter Environment Experiment data and investigated here.

References

1. G. Lange, E. Weichs, U. Schmidt, and D. Sodeikat, Spectrometer/radiometer for measurement of infrared signatures from space, *Proceedings of the SPIE-The International Society for Optical Engineering* 1340, Cryogenic Optical Systems and Instruments IV, 203-216, 1990.

2. E. Murad, D. J. Knecht, R. A. Viereck, C. P. Pike, I. L. Kofsky, C. A. Trowbridge, D. L. A. Rall, G. Ashley, L. Twist, J. B. Elgin, A. Setayesh, A. T. Stair, Jr., and J. E. Blaha, Visible light emission excited by interaction of space shuttle exhaust with the atmosphere, *Geophys. Res. Lett.* 17, 2205-2208, 1990.

3. I. L. Kofsky, D. L. A. Rall and R. B. Sluder, Measurement and interpretation of contaminant radiations in the spacecraft environment, Air Force Phillips Laboratory Technical Report TR-91-2174, June 1991, ADA241756.

4. A. L. Broadfoot, E. Anderson, P. Sherard, D. J. Knecht, R. A. Viereck, C. P. Pike, E. Murad, J. E. Elgin, L. S. Bernstein, I. L. Kofsky, D. L. A. Rall, J. Blaha, and F. L. Culbertson, Spectrographic observation at wavelengths near 630 nm of the interaction between the atmosphere and space shuttle exhaust, accepted for publication in *J. Geophys. Res.*, 1992.

5. J. B. Elgin, D. C. Cooke, M. F. Tautz, and E. Murad, Modeling of atmospherically induced gas phase optical contamination from orbiting spacecraft, *J. Geophys. Res.*, 95, 12197-12208, 1990.

6. R. A. Viereck, S. B. Mende, L. S. Bernstein, E. Murad, G. Swenson, and C. P. Pike, Visible spectra of PRCS thruster plumes, *Proceedings of the 1992 IRIS Targets, Backgrounds, and Discrimination Meeting*, 79-90, 1992.

7. I. L. Kofsky, J. L. Barrett, T. E. Brownrigg, P. J. McNicholl, N. H. Tran, and C. A. Trowbridge, Excitation and diagnostics of optical contamination in the spacecraft environment, Air Force Phillips Laboratory Technical Report AFGL-TR-88-0293, Section 5, July 1988, ADA202429.

8. H. Trinks and R. J. Hoffman, Experimental investigation of bipropellant exhaust plume flowfield, heating, and contamination and comparison with the CONTAM computer model predictions, in *Spacecraft Contamination: Sources and Prevention*, ed. J. A. Roux and T. D. McCaa, AIAA, New York, 1984.

9. L. S. Rothman, R. R. Gamache, A. Goldman, L. R. Brown, R. A. Toth, H. M. Pickett, R. L. Poynter, J. -M. Flaud, C. Camy-Peyret, A. Barbe, N. Husson, C. P. Rinsland, and M. A. H. Smith, The HITRAN database: 1986 edition, *Appl. Opt.* 26, 4058-4097, 1987.

10. M. Heninger, S. Fenistein, G. Mauclair, R. Marx, and E. Murad, Review of the reaction of O^+ with H_2O and its bearing on composition measurements from the space shuttle, Geophys. *Res. Lett.* 16, 139-141, 1989.